PAN
POLISH ACADEMY OF SCIENCES

Opto-Electronics Review

journal homepage: https://journals.pan.pl/opelre

Application of cross-correlation-based transimpedance amplifier in InAs and InAsSb IR detectors noise measurements

Krzysztof Achtenberg*, Janusz Mikołajczyk, Zbigniew Bielecki

Institute of Optoelectronics, Military University of Technology, 2 Kaliskiego St., 00-908 Warsaw, Poland

Article info

Article history:
Received 16 Feb. 2022
Received in revised form 23 Mar. 2022
Accepted 28 Mar. 2022
Available on-line 26 Apr. 2022

Keywords:
Cross-correlation; IR detector; noise; transimpedance amplifier; InAs; InAsSb.

Abstract

The paper presents noise measurements in low-resistance photodetectors using a cross-correlation-based transimpedance amplifier. Such measurements usually apply a transimpedance amplifier design to provide a current fluctuation amplification. In the case of low-resistance sources, the measurement system causes additional relevant system noise which can be higher than noise generated in a tested detector. It mainly comes from the equivalent input voltage noise of the transimpedance amplifier. In this work, the unique circuit and a three-step procedure were used to reduce the floor noise, covering the measured infrared detector noise, mainly when operating with no-bias or low-bias voltage. The modified circuit and procedure to measure the noise of unbiased and biased detectors characterized by resistances much lower than 100 Ω were presented. Under low biases, the reference low-resistance resistors tested the measurement system operation and techniques. After the system verification, noise characteristics in low-resistance InAs and InAsSb infrared detectors were also measured.

1. Introduction

Noise measurements (NMs) are practical tools to characterize many electronic devices [1, 2]. Thanks to their results, quality can be controlled and improved for appropriate interpretations of their production processes. In the case of infrared (IR) detectors, the NMs are used to determine their detectivity and provide research on new materials and structures. Remarkably, the noise appearance in biased low-resistance detectors causes a significant limitation of their detectivity at low frequencies. With generally known methods and lab equipment, measuring detector noise can be challenging compared to measuring floor noise [3–7].

The most often used systems for current noise measurements are based on a transimpedance amplifier (TIA) that converts the tested device current fluctuations into the voltage values that can be read by spectrum analyzers or acquisition systems [8]. Unfortunately, the measurements of current noise in low-resistance sources using this solution are mainly limited by the equivalent input voltage noise (EIVN) of the TIA. The noise introduced by the TIA system coming from this source grows with a decrease in the source resistance [9]. For that reason, some special circuits and solutions must be applied to obtain reliable results [10]. This paper proposes to exploit a modified cross-correlation TIA-based method that has not been tested so far with both biased and low-resistance device under test (DUT). For the first time, this method capabilities for operation with some novel optoelectronic devices: InAs and InAsSb IR detectors are demonstrated, as well.

2. Transimpedance amplifier in the noise measurements

The most known TIA circuit with a bias voltage used for noise measurements is shown in Fig. 1. It consists of the biasing source (V_B), TIA (OA_1+R_f), high-pass filter (R_1C_1), extra voltage amplifier (A_v), and a spectrum analyzer. The bias voltage (V_B) applied to the non-inverting input of the opamp forces the same voltage onto the DUT. The range of

*Corresponding author at: krzysztof.achtenberg@wat.edu.pl

https://doi.org/10.24425/opelre.2022.141126
1896-3757/ Association of Polish Electrical Engineers (SEP) and Polish Academic of Sciences (PAS). Published by PAS

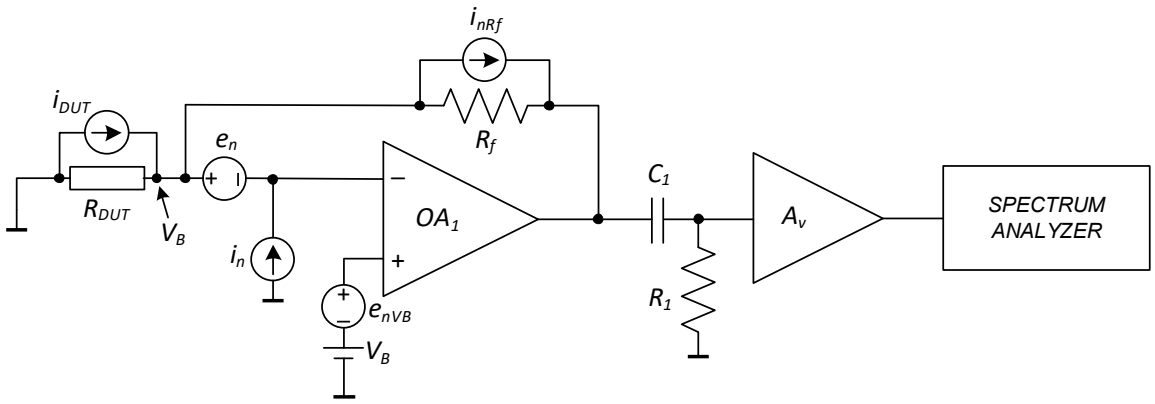

Fig. 1. The transimpedance amplifier-based noise measurement circuit.

bias voltages is limited by R_f value and maximum output voltages. The R_{DUT} is the downside resistance in the 'resistor divider' as seen by the TIA output voltage. Assuming that the primary noise comes from both TIA and biasing source (noise from AC filter and additional voltage gain stage are negligible), the power spectrum density (PSD) of the input current noise equals:

$$S_i = S_{iDUT} + S_{in} + \frac{4kT}{R_f} + S_{en}\left|\frac{1}{R_f} + \frac{1}{R_{DUT}}\right|^2 + S_{enVB}\left|\frac{1}{R_f} + \frac{1}{R_{DUT}}\right|^2, \quad (1)$$

where S_{iDUT}, S_{in}, S_{en}, and S_{enVB} are the PSDs of DUT noise, noise current, and noise voltage sources of OA_1, and noise voltage of V_B. In general terms, in the TIA, the floor noise decreases with the R_f increase. However, for $R_{DUT} << R_f$, the noise current from S_{en} and S_{enVB} becomes dominant in the overall background noise:

$$S_{iBN} \approx \frac{S_{en}}{R_{DUT}^2} + \frac{S_{enVB}}{R_{DUT}^2}. \quad (2)$$

Some current noise measurements can visualize this phenomenon. They were performed using a lab setup with some commercial instruments – TIA amplifier (5182, Signal Recovery) and FFT analyzer (SR770, Stanford Research Systems). The current noise measurements of some resistors are shown in Fig. 2. Theoretical levels of their thermal noise PSD ($4kT/R$) at 300 K were also shown to compare the expected theoretical thermal noise levels with the measured characteristics.

This setup ensures a proper noise current measurement of higher resistances (> 2 kΩ) [11]. In the case of lower resistance (below 1 kΩ), there is a need to perform an extra procedure to subtract the floor noise.

Summarizing IR detectors noise analyses with TIA-based amplifiers, some parameters of the measurement setups described in the literature are also listed in Table 1.

3. Materials and methods

As discussed in the previous section, the main limitation of providing current noise measurements in low-resistance DUTs contributes to the EIVN. For

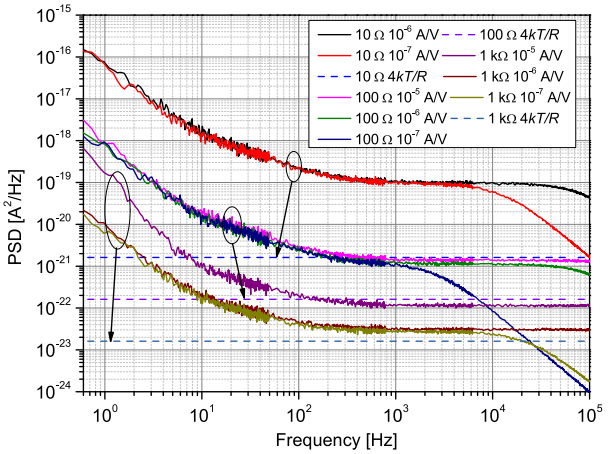

Fig. 2. Measured output noise power spectral density for 10 Ω, 100 Ω, and 1 kΩ resistor (dashed lines, $4kT/R$ – thermal noise for 300 K).

example, an EIVN of 1 nV/√Hz generates a 10 pA/√Hz extra noise for a 100 Ω DUT with a thermal noise of 12.8 pA/√Hz (300 K). This gives a value of 16.2 pA/√Hz in the 'square' sum. This result is higher by 27% than the theoretical one. This problem was analysed using the unique measurement setup proposed by G. Giusi *et al.* [12]. However, the described results concerned an unbiased 100 kΩ resistor paralleled with a 2.2 nF capacitor. Noise measurements in both biased and low-resistance DUT (R < 100 Ω) become the main issue of this work. They are the key issue in the characterization of novel IR detectors. Let us describe the operating procedures of a modified two-channel amplifier with a photodiode (PD) (Fig. 3). In this circuit, a biasing source was connected to the non-inverting inputs of a two-channel differential TIA. Each channel was also equipped with buffers and high-pass filters. The applied TIA construction was described in Ref. 12. The measurements conditions were set with some switches. This allows, e.g., to connect a PD cathode to the inverting input of each channel and force the reverse bias condition. For non-biasing conditions, the measurement setup is commonly known (SW_3, SW_4 – position 2). The design has been changed for the biased PD. During these measurements, the PD cathode is connected to the OA_1 and its anode to the ground (SW_5 – position 1, SW_1 – position 1, SW_2 – position 2). The bias voltage applies to the non-inverting input of the OA_1 (SW_3 – position 1, SW_4 – position 2).

Table 1.
Performances of some IR detectors current noise measurements with TIA.

Type of the measured detectors*	Detector resistances	Model of the front-end	Measurement system noise (amplifiers)	Measurement bandwidth**	Range of bias (rev.)	Ref.
HgCdTe, InAs/GaSb T2SL	≈ 60 Ω to above 1 MΩ (dynamic resistance)	TIA EG&G 5182	$e_n = 1\times10^{-17}$ V²/Hz at 100 Hz $i_n = 2\times10^{-27}$ A²/Hz [10^8 V/A] at 1 kHz $i_n = 2\times10^{-24}$ A²/Hz [10^6 V/A] at 1 kHz	1 Hz to 10 kHz	1.5 mV to 1 V	[11]
InAs/GaSb SL	$R_0A = 5.3\times10^5$ Ωcm² at [80 K]	TIA Keithley 428	$i_n = 90$ nA$_{rms}$ at 10^3 V/A $i_n = 1.2$ fA$_{rms}$ at 10^{11} V/A	0.3 to about 200 Hz	100 to 800 mV	[13]
InAs/GaSb SL	R_0A higher than 1×10^6 Ωcm² at [77 K]	TIA DDPCA-300	$i_n = 2\times10^{-21}$ A²/Hz [10^4 V/A] at 10 Hz $i_n = 4\times10^{-30}$ A²/Hz [10^{12} V/A] at 10 Hz	1 to 20 Hz	0.2 to 0.9 V	[14]
InAs/GaSb SL	–	TIA DLPCA-200	$e_n = 1.6\times10^{-17}$ V²/Hz at 1 kHz $i_n = 4\times10^{-22}$ A²/Hz [10^3 V/A] at 10 kHz $i_n = 1.85\times10^{-29}$ A²/Hz [10^{11} V/A] at 100 Hz	1 to 800 Hz	0.05 to 0.8 V	[15]
PbS (photo-conductor)	≈ 60 kΩ to 5 MΩ	TIA DLPCA-200	$e_n = 1.6\times10^{-17}$ V²/Hz at 1 kHz $i_n = 4\times10^{-22}$ A²/Hz [10^3 V/A] at 10 kHz $i_n = 1.85\times10^{-29}$ A²/Hz [10^{11} V/A] at 100 Hz	500 Hz to 5 kHz	2 to 6 V	[16]
HgCdTe	$R_0A = 4.6\times10^7$ Ωcm²	Custom Design TIA (CD) or SR570	$e_n = 3.6\times10^{-17}$ V²/Hz* $i_n = 1.7\times10^{-30}$ A²/Hz [< 10 Hz] (CD) $e_n \approx 1\times10^{-17}$ V²/Hz at 1 kHz $i_n = 3.6\times10^{-29}$ A²/Hz [10^9 V/A] at 1 Hz (SR570)	0.1 Hz to 2 kHz	10 to 300 mV	[17]

*data from VISHAY 2N4416 JFET datasheet

**the frequency range in which the measurements were performed

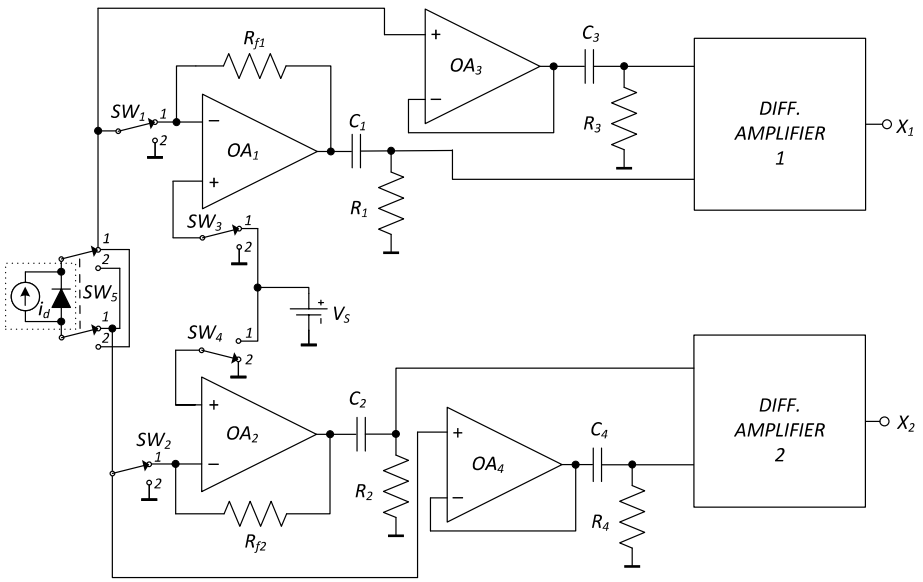

Fig. 3. The scheme of the proposed circuit to measure current noise in biased low-resistance DUTs.

The inverting input of the OA_2 is open. Assuming the noise from additional buffers is negligible, PSD obtained at the X_1 output is [12]:

$$S_1 = (S_{en1} + S_{enVB}) \left| \frac{1}{R_{f1}} + \frac{1}{R_D} \right|^2 + S_{in1} + S_{iRf1} + S_{id}\,, \quad (3)$$

where S_x are the x-source PSD contributions from detector noise (i_d), both equivalent input current and voltage noises (i_{n1}, i_{n2}, e_{n1}, e_{n2}) from each differential channel (OA_1 and OA_2), and the biasing source noise e_{nVB}.

In the next step, the connection scheme is the same with the second measurement channel (SW_5 – position 2, SW_1 – position 2, SW_2 – position 1, SW_3 – position 2 and SW_4 – position 1). The PSD expression of the signal X_2 is:

$$S_2 = (S_{en2} + S_{enVB}) \left| \frac{1}{R_{f2}} + \frac{1}{R_D} \right|^2 + S_{in2} + S_{iRf2} + S_{id}\,. \quad (4)$$

During the last procedure step, the tested PD is connected to both amplifiers (OA_1 and OA_2) (SW_5 – position 1, SW_1 – position 1, SW_2 – position 1) with the biasing voltage at the OA_1 (SW_3 – position 1, SW_4 – position 2). It still provides the reverse-biasing of the PD. The PSDs of output voltages X_1 and X_2 are:

$$S_{11} = (S_{en1} + S_{en2} + S_{enVB}) \left| \frac{1}{R_{f1}} + \frac{1}{R_D} \right|^2 + S_{in1} + S_{iRf1} + S_{id} \quad (5)$$

and

$$S_{22} = (S_{en1} + S_{en2} + S_{enVB}) \left| \frac{1}{R_{f2}} + \frac{1}{R_D} \right|^2 + S_{in2} + S_{iRf2} + S_{id}\,. \quad (6)$$

The cross-spectrum of these signals is given by:

$$S_{12} = -\left(S_{id} + (S_{en1} + S_{enVB}) \left| \frac{1}{R_{f1}} + \frac{1}{R_D} \right|^2 + S_{en2} \left| \frac{1}{R_{f2}} + \frac{1}{R_D} \right|^2 \right). \quad (7)$$

These equations extract the noise generated by the tested device (photodetector) with:

$$S_{id} = -S_{12} - (S_{11} - S_1) - (S_{22} - S_2) - S_{enVB} \left| \frac{1}{R_{f1}} + \frac{1}{R_D} \right|^2, \quad (8)$$

where R_D is the detector resistance.

The described method minimizes the influence of amplifiers (opamps) noise sources. And the impact of the biasing source noise depends on the PD resistance (the higher resistance, the lower impact). These considerations, however, are valid for some assumptions, e.g., uncorrelation of amplifiers noise sources (e_{n1}, e_{n2}, i_{n1}, i_{n2}) and well-characterized noise introduced by the low-noise biasing source (S_{enVB}) because this component must be individually subtracted. This value was measured to validate the final experiment results.

4. Experimental validation

Authors' experiments tested the described measurement setup with two different amplifier configurations of OA_1 and OA_2 (OP27G and LT1028A opamps). OA_3 and OA_4 buffers were built with low-noise JFETs inputs ADA4625. This opamp also provides a low voltage noise of 3.3 nV/√Hz at 1 kHz. Metalized polyester capacitors (3.3 µF) and metalized resistors (200 kΩ) designed AC-high pass filters. The 'DIFF. AMPLIFIER' amplifiers constructed with TLC071 and OP27G opamps provide a 101 V/V gain. The biasing voltage was supplied using a low-noise programmable voltage source with JFETs described in Ref. 18. An example of its noise characteristics is presented in Fig. 4.

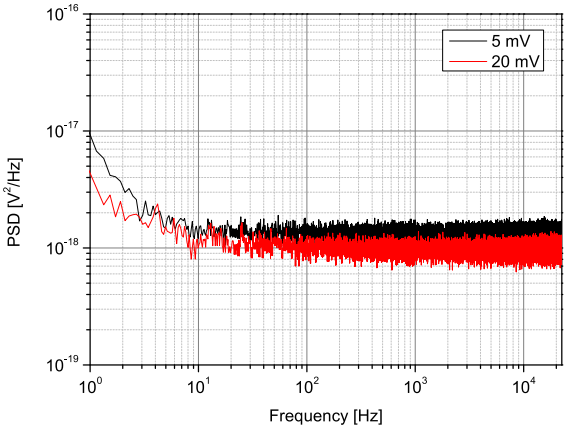

Fig. 4. The PSDs of the bias voltage source – S_{enVB}.

All measurement components were placed into a special mumetal-shielding chamber with isolated BNCs connectors. The 24-bit data acquisition card PCI-4462 (National Instruments) with anti-aliasing filters digitizes all signals. The PSDs calculation procedure was processed using MATLAB software. A 50 kS/s acquisition frequency, 20 minute time of averaging spectra in cross-correlation, and 2^{14} FFT points were set during the measurements. Such parameters yield 3662 averages.

Noise measurements of well-known resistors checked the setup performance, defining noise measurement ability in low resistances. The influence of opamp noise parameters during the preliminary tests were determined. The first one was the OP27G opamp ($e_n = 3$ nV/√Hz, $i_n = 0.4$ pA/√Hz at 1 kHz) with a 1 kΩ feedback resistance (R_f). The results of current noise measurements in unbiased resistors are presented in Fig. 5 (for 1 kΩ and 100 Ω) and in Fig. 6 (for 10 Ω and 51 Ω).

Application of OP27G opamps allows current noise measurements of both 1 kΩ and 100 Ω resistances. The results referring to a single-channel ($S1$ result) are a few times higher than the extracted DUT noise. Also, the two-channel cross-correlation ($S12$) is insufficient to obtain the similar effect. Some differences are noticed due to the change of the noise voltage gain characteristics and the increased value of the EIVN ($1/f$ region) for 51 Ω and 10 Ω. The observed noise underestimation level is caused by a reduced transimpedance gain (unstable TIA), and the subtraction procedure generates deviations at higher level signals for lower resistances.

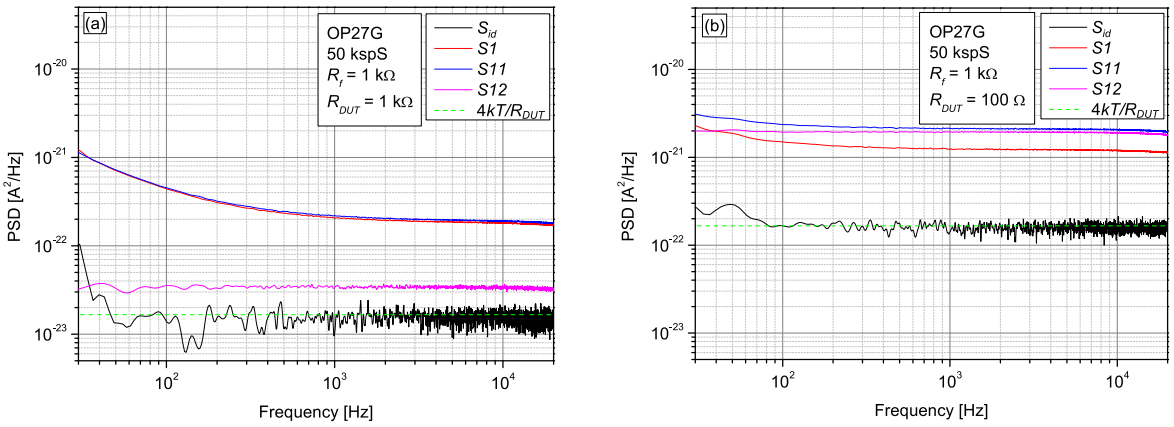

Fig. 5. Current noise measurements in 1 kΩ (a) and 100 Ω (b) unbiased resistors at 300 K with OP27G opamps.

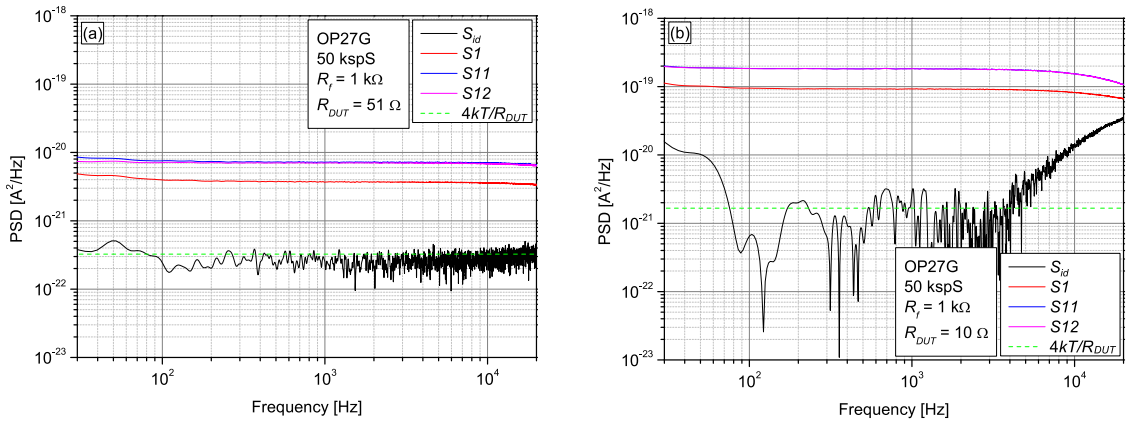

Fig. 6. Current noise measurements in 51 Ω (a) and 10 Ω (b) unbiased resistors at 300 K with OP27G opamps.

In the next step, an ultra-low noise opamp LT1028A was used. It has a voltage noise of 0.85 nV/√Hz, current noise of 1 pA/√Hz at 1 kHz, and a gain-bandwidth product of 50 MHz. The current noise measurements in the identical resistors are shown in Fig. 7 and Fig. 8. It allows for result corrections of resistances below 100 Ω. For example, the thermal noise was extracted with an error of 2% in a 51 Ω resistor. Compared to the OP27G, a lower influence of EIVNs of OA_1 and OA_2 was observed. The same error level occurs for a lower resistance of 10 Ω. Some results for different measurement times in the range from 10 s (30 averages) to 20 min (3662 averages) were also shown in Fig. 9. The 51 Ω resistor has no strong time range influence on the PSD level. In the case of 1 kΩ, the result obtained at 10 s (2.71×10^{-23} A²/Hz) is higher by 68% than the result obtained (1.68×10^{-23} A²/Hz) at 20 min. This phenomenon was observed for the 1 kΩ resistors due to the feedback resistance noises (the same current noises of feedback resistors compared to the DUT) which are reduced by cross-correlation. The obtained results also indicate that the measurement time influences the standard deviation of the PSD result characteristics. It sets the number of averages which can be done in the measurement time with a desired FFT resolution.

The authors performed some measurements of the biased resistors to visualize the influence of the biasing source noise on the calculated spectrum. According to (2), this should be visible in a low-resistance DUT. In Fig. 10(a), an increase in the PSD noise for a 51 Ω resistor (1 nV/√Hz voltage noise equals ≈ 20 pA/√Hz) was observed. For a 1 kΩ resistor, there are no essential changes [Fig. 9(b)]. Additionally, the results obtained for the 5 mV biasing are higher than for the 20 mV biasing due to the higher noise of the applied voltage source. This experiment confirms the neccessity of the voltage source subtraction during noise measurements of low-resistance devices as in (8). To determine the error of the obtained results, 10 measurements of the noise voltage source set at 20 mV and 10 measurements of the biased 51 Ω resistor were performed. The estimation error of the thermal noise was about 7%. The standard deviation of the results was about 10^{-23} [A²/Hz].

5. InAs and InAsSb IR detectors noise measurements

The main research task was to measure the noise characteristics of two low-resistance photodetectors at different biasing. The first one was the InAs IR detector with a resistance of about 80 Ω at 300 K (no-biased), an active area of 1×1 mm, and an optimized wavelength of 3.4 µm. The second sample was an InAsSb detector optimized for a wavelength of 5 µm with a 70 Ω resistance of about 300 K (no-biased), an active area of 0.1×0.1 mm. The tested detectors were mounted on a specially prepared socket and radiator. The setup with LT1028A opamps was

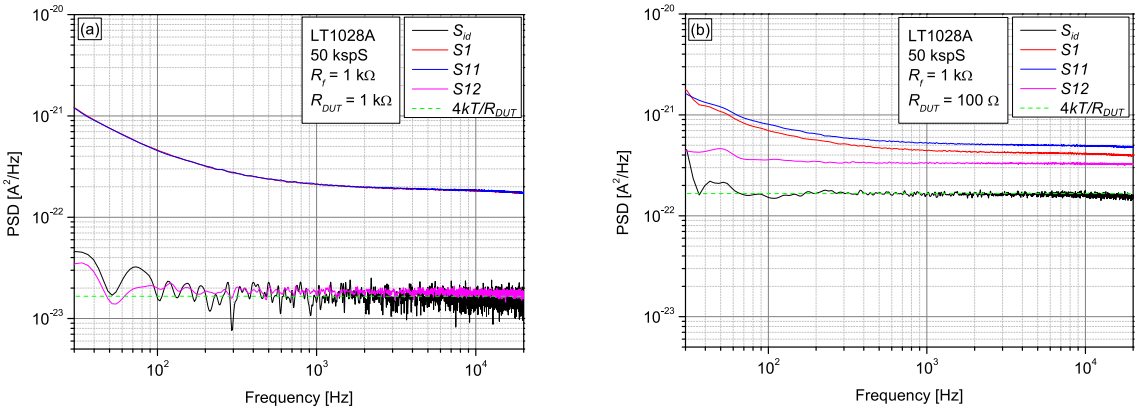

Fig. 7. Current noise measurements in 1 kΩ (a) and 100 Ω (b) unbiased resistors

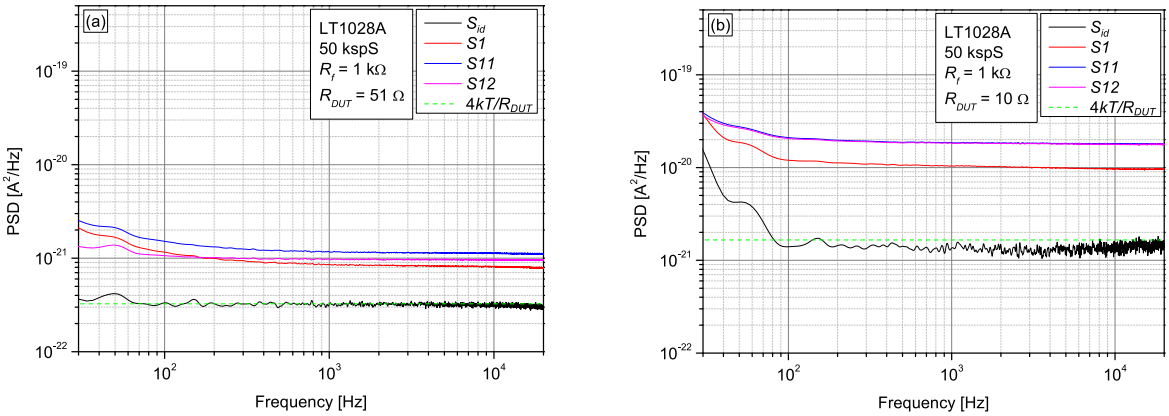

Fig. 8. Current noise measurements in 51 Ω (a) and 10 Ω (b) unbiased resistors at 300 K with LT1028A opamps.

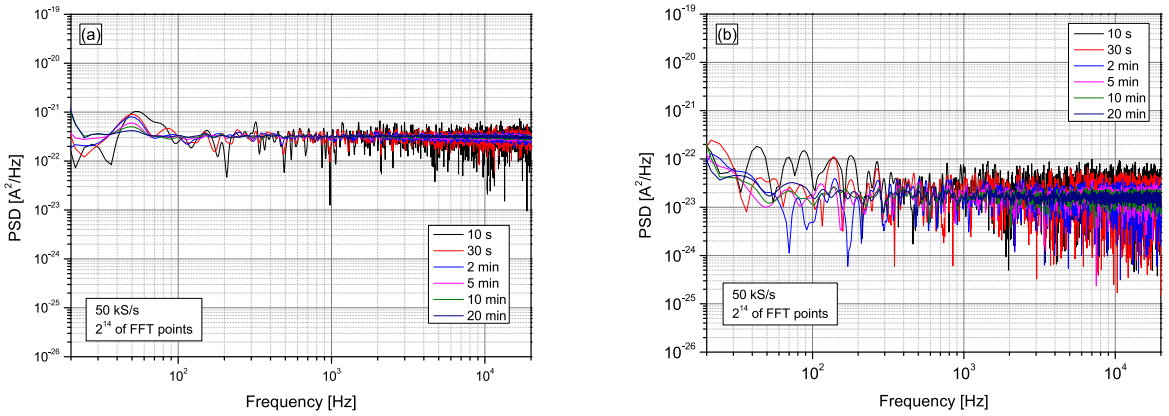

Fig. 9. Current noise measurements in 51 Ω (a) and 1 kΩ (b) resistors at 300 K with LT1028A opamps for different averaging times.

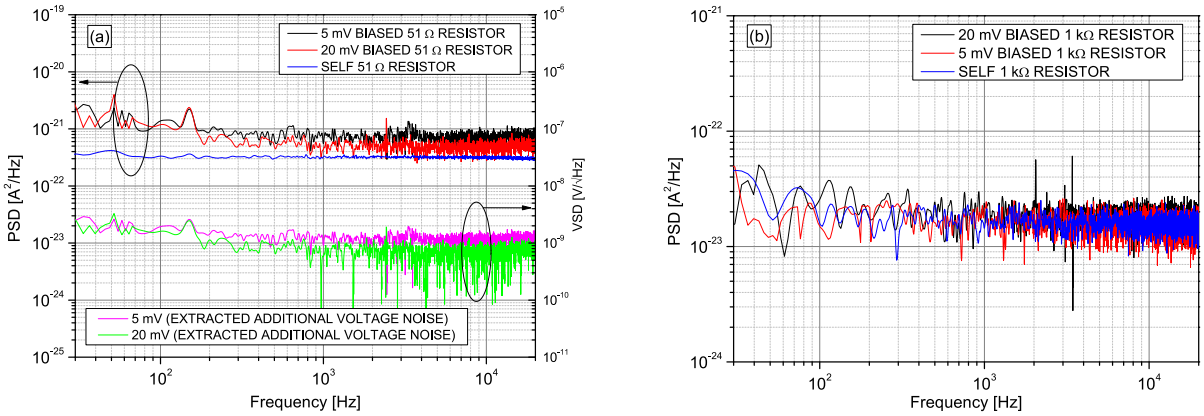

Fig. 10. Current noise measurements of biased 51 Ω (a) and 1 kΩ (b) resistors at 300 K with LT1028A opamps.

applied as a better measurement tool considering detectors resistances. There are some measured noise spectra for the unbiased detectors presented in Fig. 11. Some external interferences cause a bump near 50 Hz. The mV range biasing was selected to estimate $1/f$ noise. Some results are presented in Fig. 12 and Fig. 13 for InAs and InAsSb, respectively. The described setup has some advantages when comparing the signals of $S1$, $S12$, and S_{id}. However, it should be noticed that the voltage noise of the biasing source depends on the output voltage level and it increases as the output voltage decreases. Moreover, the biasing voltage causes an increase in the detector resistance. As a result, the 'white noise' level for a 5 mV-biased InAs detector is higher than that obtained for a 20 mV-biased one (Fig. 12). In the case of InAsSb (Fig. 13), these phenomena are less distinct due to a higher $1/f$ noise level (frequency range). It should be emphasized that these measurements are challenging because of the limited noise performances of the biasing source. For example, a biasing source noise of 1×10^{-18} V^2/Hz generates an extra noise of 1.56×10^{-22} A^2/Hz at a 80 Ω resistance of the InAs detector. For this reason, current noises of the biasing source for 5 mV and 20 mV voltage levels were also determined considering actual detector resistance (R_{det}).

The calculation results present the characteristics of the current noise due to the voltage source (S_{inVB}) as the ratio

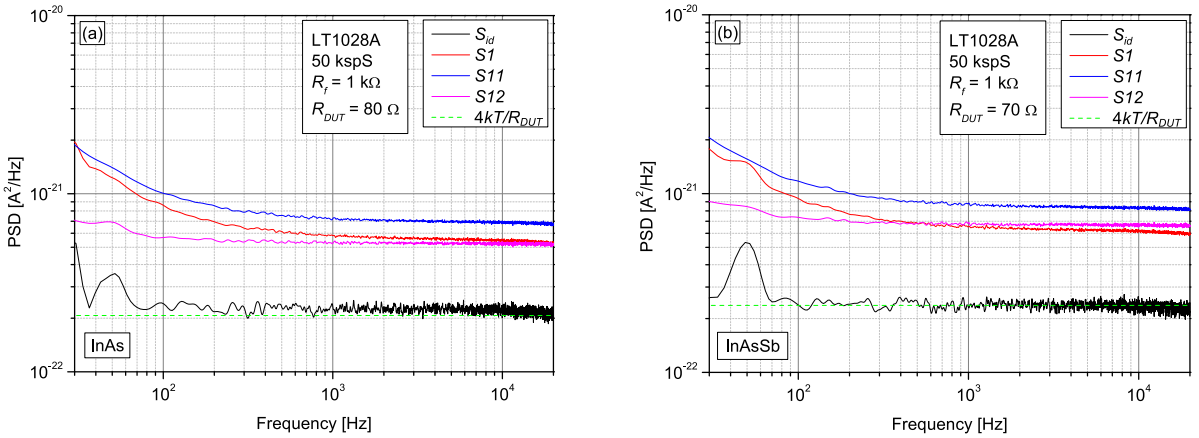

Fig. 11. Results of current noise measurements in unbiased InAs (a) and InAsSb (b) detectors at 300 K.

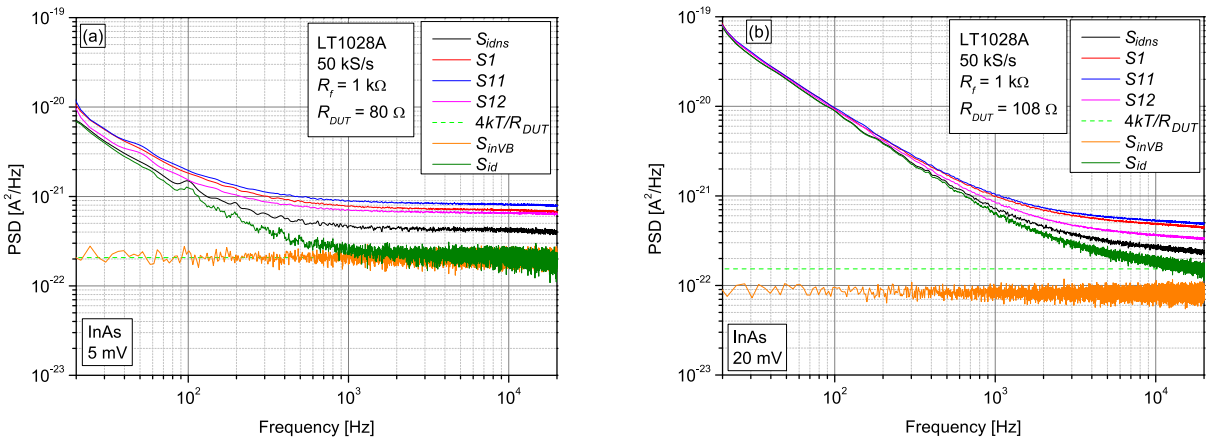

Fig. 12. Results of current noise determination in the InAs detector at 300 K with a reverse biasing of: 5 mV (a) and 20 mV (b).

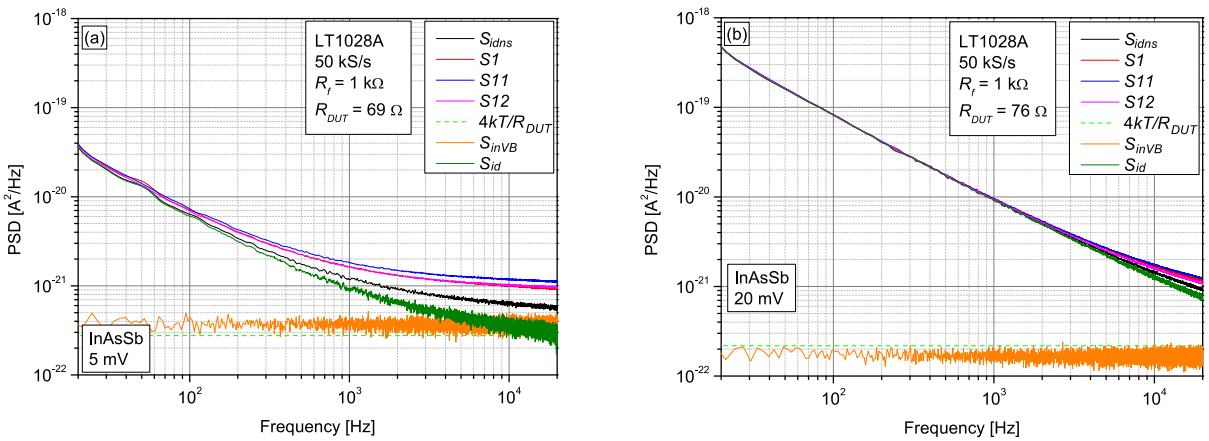

Fig. 13. Results of current noise measurements in the InAsSb detector at 300 K with a reverse biasing of: 5 mV (a) and 20 mV (b).

of $S_{enVB}/(R_f \| R_{det})^2$, the detector current noise without voltage source noise subtraction (S_{idns}), and the final detector noise with biasing noise subtraction (S_{id}).

6. Conclusions

This paper presents instrumentation that provides current noise measurements in biased low-resistance IR detectors. Described tools allow the estimation of a device noise with a low-floor noise. It was obtained by combining the method based on a two-channel cross-correlation TIA and a three-step measurement procedure. Some modifications of amplifiers allow the noise measurements in low-resistance and biased devices. Performance of this design was tested by measuring the current noise in some reference resistors. Finally, the results of current noise measurements in InAs and InAsSb IR detectors were also presented.

Authors' statement

Research concept and design, K. A.; collection and assembly of data, K. A.; data analysis and interpretation, K. A, J. M., Z. B.; writing the article, K. A., J. M.; critical revision of the article, J. M., Z. B.; final approval of the article, Z. B.

References

[1] Vandamme, L. K. J. Noise as a diagnostic tool for quality and reliability of electronic devices. *IEEE Trans. Electron. Devices*. **41**, 2176–2187 (1994). https://doi.org/10.1109/16.333839

[2] Kotarski, M. M. & Smulko, J. M. Noise measurement set-ups for fluctuations-enhanced gas sensing. *Metrol. Meas. Syst*. **16**, 457–464 (2009). http://www.metrology.pg.gda.pl/full/2009/M&MS_2009_457.pdf

[3] Jones, B. K. Electrical noise as a reliability indicator in electronic devices and components. *IEE Proc. G* **149**, 13–22 (2002). https://doi.org/10.1049/ip-cds:20020331

[4] Dyakonova, N., Karandashev, S. A., Levinshtein, M .E., Matveev, B. A. & Remennyi, M. A. Low frequency noise in p-InAsSbP / n-InAs infrared photodiodes. *Semicond. Sci. Technol*. **33**, 065016 (2018). https://doi.org/10.1088/1361-6641/aac15d

[5] Ciura, L., Kolek, A., Michalczewski, K., Hackiewicz, K. & Martyniuk, P. 1/f noise in InAs/InAsSb superlattice photoconductors. *IEEE Trans. Electron Devices*. **67**, 3205–3210 (2020). https://doi.org/10.1109/TED.2020.2998449

[6] Savich, G. R., Pedrazzani, J. R., Sidor, D. E., Maimon, S. & Wicks, G. W. Dark current filtering in unipolar barrier infrared detectors. *Appl. Phys. Lett.* **99**, 121112 (2011). https://doi.org/10.1063/1.3643515

[7] Cervera, C. *et al*. Dark current and noise measurements of an InAs/GaSb superlattice photodiode operating in the midwave infrared domain. *J. Electron. Mater.* **41**, 2714–2718 (2012). https://doi.org/10.1007/s11664-012-2035-4

[8] Ciofi, C., Giusi, G., Scandurra, G. & Neri, B. Dedicated instrumentation for high sensitivity, low frequency noise measurement systems. *Fluct. Noise Lett.* **4**, L385–L402 (2004). https://doi.org/10.1142/S0219477504001963

[9] Horowitz, P. & Hill, W. *The Art of Electronics* (Cambridge University Press, 2015).

[10] Achtenberg, K. *et al*. Low-frequency noise measurements of IR photodetectors with voltage cross correlation system. *Measurement* **183**, 109867 (2021). https://doi.org/10.1016/j.measurement.2021.109867

[11] Ciura, Ł., Kolek, A., Gawron, W., Kowalewski, A. & Stanaszek, D. Measurements of low frequency noise of infrared photodetectors with transimpedance detection system. *Metrol. Meas. Syst.* **21**, 461–472 (2014). https://doi.org/10.2478/mms-2014-0039

[12] Giusi, G., Pace, C. & Crupi, F. Cross-correlation-based trans-impedance amplifier for current noise measurements. *Int. J. Circ. Theor. Appl*. **37**, 781–792 (2008). https://doi.org/10.1002/cta.517

[13] Jaworowicz, K., Ribet-Mohamed, I., Cervera, C., Rodriguez, J. B. & Christol, P. Noise characterization of midwave infrared InAs/GaSb superlattice pin photodiode. *IEEE Photon. Technol.* **23**, 242–244 (2011). https://doi.org/10.1109/lpt.2010.2093877

[14] Taalat, R., Christol, P. & Rodriguez, J. Dark current and noise measurements of an InAs/GaSb superlattice photodiode operating in the midwave infrared domain. *J. Electron. Mater.* **41**, 2714–2718 (2012). https://doi.org/10.1007/s11664-012-2035-4

[15] Ramos, D. *et al.* 1/f noise and dark current correlation in midwave InAs/GaSb Type-II superlattice IR detectors. *Phys. Status Solidi A.* **218**, 2000557 (2020). https://doi.org/10.1002/pssa.202000557

[16] De Iacovo, A., Venettacci, C., Colace, L. & Foglia, S. Noise performance of PbS colloidal quantum dot photodetectors. *Appl. Phys. Lett.* **111**, 211104 (2017). https://doi.org/10.1063/1.5005805

[17] Rais, M. H. *et al*. HgCdTe photovoltaic detectors fabricated using a new junction formation technology. *Microelectron. J.* **31**, 545–551 (2000). https://doi.org/10.1016/s0026-2692(00)00028-8

[18] Achtenberg, K., Mikołajczyk, J., Ciofi, C., Scandurra, G. & Bielecki, Z. Low-noise programmable voltage source. *Electronics* **9**, 1245 (2020). https://doi.org/10.3390/electronics9081245